J. Bangladesh Acad. Sci. 50(1); 23-34: March 2026 DOI:https://doi.org/10.3329/jbas.v50i1.84634

Journal of Bangladesh Academy of Sciences

Journal homepage: http://www.bas.org.bd/publications/jbas.html

Research Article

A comparative study on flow-induced phenomena of servo-valve for realizable $k-\varepsilon$ and spalart-allmaras turbulence model under malfunction

Md. Shah Najmus Shakib[1] and Bijan Krishna Saha[*]

Department of Mathematics, Faculty of Science, University of Barishal, Barishal, Bangladesh

ARTICLE INFO

Article History

Received: 28 September 2025
Revised: 27 January 2026
Accepted: 29 January 2026

Keywords: Deflector jet servo-valve (DJSV), Computational fluid dynamics (CFD), Electro-hydraulic servo-valve (EHSV), Pressure and flow distribution, Cavitation.

ABSTRACT

Servo-valves are widely used in the aerospace, mechanical, and aeronautics sectors, where precise control of missile fins and aircraft components is essential. This study presents a details comparison between the Realizable $k-\varepsilon$ turbulence model and the Spalart-Allmaras turbulence model to evaluate flow behavior and its impact on servo-valve malfunction. This article highlights the critical role of electrohydraulic servo-valves in ensuring the performance and reliability of the servo control systems. Computational fluid dynamics (CFD) is employed to analyze pressure distribution, velocity patterns, and flow behaviors within the pilot stage of the servo-valves. Additionally, mesh refinement techniques are applied to achieve optimal accuracy and computational efficiency in capturing flow physics. Significant variations in pressure and velocity fields are observed, demonstrating the differing predictive capabilities of the turbulence models in capturing flow-induced effects. Therefore, this study provides valuable insights for improving servo-valve design and mitigating performance degradation caused by flow-related malfunctions..

Introduction

The EHSV affects the efficiency and dependability of the servo control system and is among the most prone parts to malfunction. For cost and performance, Tamburrano et al. (2018) assessed computational fluid dynamics analysis of electro-hydraulic servo-valves, novel control strategies, and smart material combinations. Because of its excellent contamination resistance, rapid dynamic response, improved flow control, and dependability, DJSV is used in many technological fields. Conversely, flow cavitation arising from the dynamic and static performance of the deflector jet servo-valve could compromise the accuracy of the hydraulic servo control system. It generates power loss, vibration, noise, and component deterioration of hydraulic valves. In a water-hydraulic valve, Liang et al. (2016) examined input pressure variations and unstable cavitation conditions. Their results showed that while a groove at the port of the valve can minimize cavitation severity during initial pressure changes, raising or lowering the frequency can help diminish cavitation enhancement. For a water poppet valve, Han et al. (2017) computed the cavitation and flow force. Their results revealed that valve cavitation can be avoided with a special valve-opening and outlet-pressure arrangement. A spool valve having U-grooves showed more severe cavitation as the valve opening and groove depth increased, claims Zou et al. (2008). Investigating the vortex and flow stream during metering in a spool valve with varying valve apertures, Gao (2009) used finite element and PIV approaches. Chen et al. (2019) sought the source of self-excited noise in the flapper-nozzle servo-valve pilot stage. Numerical models and experimental flow

[*]Corresponding author: <bksaha@bu.ac.bd>

[1]*Department of Mathematics, University of Global Village (UGV), Barishal, Bangladesh*

data suggest that the cavitation increases as oil viscosity decreases. Their studies also showed that noise was produced by unstable cavitation in the pilot stage. Other studies, in the meantime, studied the directional control valve and servo-valve spool pressure losses and flow characteristics using numerical simulations. Using pure water flowing through the valve port, Zhang et al. (2012) focused on energy loss, cavitation erosion, and spiral vortices. Sandor and Suan-Resiga found that more severe and destructive cavitation followed by increased input pressure (Sandor and Suan-Resiga, 2012). The flow profile and cavitation events within hydraulic servo-valve pilot stages have been investigated theoretically and experimentally on several occasions. The pilot-stage flow field of a dual nozzle-flapper servo-valve was investigated by Jacob et al. (2011) using CFD. They demonstrated the stability of the conventional turbulence model for incompressible steady fluid flow profile in a servo-valve pilot stage. Li et al. (2013) assessed cavitation in the pilot stage of a flapper-nozzle servo-valve at Reynolds numbers between 630 and 2500. Also, the hollow, cloud-like shape on the flapper's curved surface was examined. Aung and Li (2014) designed a special rectangular flapper form to prevent cavitation. The efficiency of the new flapper form was shown by its identical flow characteristics to those of the traditional flapper form. Using three flapper geometries, Yang et al. (2015) examined cavitation effects under four flow conditions and changing input pressures with two flapper-nozzle null clearances (0.2 mm and 0.1 mm). The researchers found that in the pilot valve, flutter-nozzle null clearance and intake pressure improved turbulent jets and cavitation. Finally, rectangular flappers reduce cavitation between the pilot valve and the flapper nozzle. Several researchers have recently examined electrohydraulic servo-valve cavitation to improve pilot-stage performance. Yang et al. (2019a) studied cavitation reduction using microjets surrounding the main jets of the flapper-nozzle servo-valve. Their results showed that continuous micro-jets greatly decreased flapper-nozzle valve cavitation. Yang et al. (2019b) investigated the flapper-nozzle pilot stage cavity and flow forces in a hydraulic servo-valve at multiple supply pressures using continuous microjets. To avoid cavitation in the nozzle-flapper servo-valve, Yang et al. (2019c) argued for replacing circular nozzles with diamond ones. They found that, in numerical simulations, a modified nozzle structure might reduce cavitation without compromising servo-valve performance. Wu et al. (2018) investigated cavitation intensity using LES and snapshots. The results revealed that whilst raising the deflection angle stabilizes the flow field, increasing the jet pipe input pressure generates turbulent components with smaller vortices. Using two usually closed two-way two-position valves operated by two piezoelectric ring benders, Tamburrano et al. (2020) created a pilot stage flapper-nozzle servo-valve to control quiescent flow when the main stage is stationary. Numerical models and experiments are compared to guarantee consistent findings. The model-based work of Ren et al. (2022) on servo-values validated the hypotheses of jet theory about the design of the deflector jet valve. Emphasizing the importance of inlet pressure on performance, Abdallah et al. (2023a) examined pressure oscillation and structural factors.

To better grasp the internals of the deflector jet servo-valve, Yan et al. (2019) created a computational model. Additionally, Abdallah et al. (2023b) examined erosion events. They advised performance improvements and focused on the shunt wedge. Chu et al. (2021) examined oil-contaminated performance degradation with multi-physics simulation correction and theoretical analysis. To maximize jet-pipe servo-valve dynamics, Chen et al. (2022) applied a mathematical model and a hierarchical particle swarm optimization genetic technique. The dynamic erosion wear of the nozzle flapper pressure servo-valve of an aircraft braking system was investigated in another paper by Chu et al. (2020). Yan et al. (2020) quantitatively investigated erosion wear in a hydraulic amplifier of a deflector jet servo-valve and derived failure criteria and a lifespan prediction formula depending on hydraulic oil contamination.

Electrohydraulic servo-valves are an inseparable element of systems in the aerospace, automotive, and industrial sectors, where hydraulic fluids are controlled to ensure processes run smoothly and with accuracy. However, typical deviations include irregular flow and pressure fluctuations, which occur due to malfunctions and thereby affect the performance of the whole system, leading to complete failure. A thorough understanding of these concerns forms a decisive part of the quest to increase the reliability and efficiency of the servo-valve.

While previous studies have extensively examined turbulence models, including the Realizable $k-\varepsilon$ and Spalart-Allmaras models in general nozzle flows or convergent-divergent jets, a direct comparison with electro-hydraulic servo-valves, especially deflector-jet systems under conditions of malfunction, is evidently lacking. As a result, measurements of model-specific predictions applicable to pilot-stage reliability are restricted. The vast majority of previous research has focused on valves in an ideal, neutral state or during steady-state erosion, leaving an essential knowledge gap about the behavior of turbulence models in the presence of an asymmetric pressure gradient and local flow separation caused by the physical misalignment. When the flapper is positioned in the middle position, the flow is symmetric. However, when the flapper is misaligned due to mechanical failure or excessive use, the flow becomes assymmetric. In that case, it requires the comparative use of two models as it transforms this stable jet into a highly non-linear flow field.

This paper attempts to fill this gap by proposing a rotational malfunction as an exemplar of a failure mode, thereby providing a more general model for considering valve reliability under non-ideal mechanical conditions. The study compares the Spalart-Allmaras and realizable $k-\varepsilon$ models in a deflector jet servo-valve (DJSV) under malfunction and reveals distinct changes in the pressure and velocity fields, which guide optimal model selection to enhance the reliability of the valve in high-pressure aerospace applications. A 5-degree rotation is used to induce significant changes in flow behavior, with smaller angles yielding trivial changes that cannot allow a sound conclusion.

The essence of the study phenomenon is its coverage of this gap by clarifying the effect of model choice on predicting changes in flow components caused by malfunctions and by complying with the practical imperative to gain accessy to efficient servo-control apparatus in areas that indeed demand precision. The findings can be used to design better valves in conditions where the valve malfunctions, as they identify the type of turbulence model that better reflects the flow phenomena. At the same time, as a practical application of improvement, the research is expected to enhance the efficiency and reliability of critical systems that utilize servo-valves.

Operating principle and flow field

As shown in Fig. 1, a two-stage deflection flapper servo-valve typically has a pilot and main stage. Electromagnetic torque drives the pilot stage. As an electromechanical converter, the motor and hydraulic amplifier ensure proper movement of the main stage (spool) and proper performance of the pilot stage. The amplifier jet disk is established, and a deflection flapper with a V-shaped guiding groove is meticulously placed between the supply nozzle and two receiving ports during the pilot stage. Fig. 1 shows the amplifier disk and deflection flapper in close-up. Its term is considered as coil current. A slight current applied to the electromagnetic torque motor induces the flapper to rotate at a limited angle.

From the fixed intake, the flapper grooves direct fluid flow to one of two receiving ports. The main spool in the port is driven in the opposite direction to the flapper's movement by a pressure difference created there. The feedback rod links the flapper and spool to balance forces. The flapper is in the null state when the torque motor voltage is zero, therefore dispersing fluid equally between two receiving ports from the supply nozzle. Should both receiving ports

have the same energy consumption, the pressure differential between them will be zero (Saha et al., 2020). Further, for rotational movement of the servo-valve, the valve's components include a rotary actuator, rotary wheel, rotary flapper, receiver ports, and a supply nozzle. The rotary actuator generates electrical torque that drives the flapper to rotate. The fluid goes to the receiving ports, which regulate the main stage flow in the valve. To provide precise control, a feedback rod connects the flapper to the spool. Rotational motion reduces damage and improves control precision, hence allowing small, long-lasting devices (Saha et al., 2024).

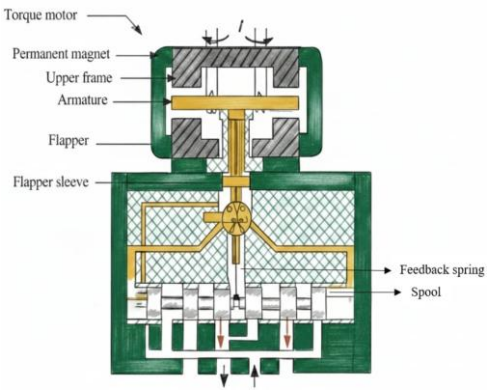

Fig. 1. Schematic of a two-stage deflection flapper servo-valve with pilot and main stage.

Execution of CFD analysis

The implementation of this numerical analysis is based on the coupling of mechanical failure suppositions and the resulting fluid-structure interaction. One of the fundamental assumptions of this study is that the deflector jet undergoes a 5-degree rotational malfunction under non-linear operating conditions. Physically, such a condition requires a specialized model formulation to capture the intricate flow phenomena.

A. Simplification of geometric models

As seen in Fig. 2, the flow channel inside the initial stage of the servo-valve has a complex geometry. Fig. 2(a) shows the amplifier disk, and Fig. 2(b) shows the CAD model of this study.

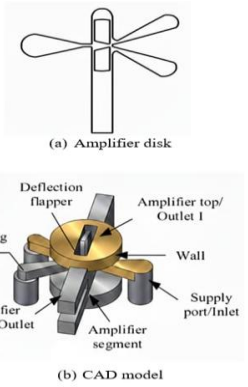

(a) Amplifier disk (b) CAD model

Fig. 2. Computational domain of the flapper pilot stage.

The dimensions of the amplifier disk for this study are based on the model developed earlier by Saha et al. (2020). By limiting the simulation to the nearest part of the pilot stage, we may improve computing performance and conserve memory.

B. Grid independence test

Mesh quality in CFD simulations has a significant impact on the numerical solution to a specific problem. Three distinct grid sizes, Grid E, Grid F, and Grid G, are used for the validation of the grid. It is abundantly evident that numerical convergence with numerous grids has significant obstacles. Using many grids, the surface average for both models is approximated to explore the dependency of the grid on the simulation results, as given in Table 1. Grid E and Grid F have a relative error of less than 3%; Grid F and Grid G have less than 2%. Grid F is employed in this study for numerical simulations to compromise computational expense with numerical accuracy.

Table 1. Findings from the grid independence test.

Grid	Cells	Faces	Vertices	Surface average (Realizable k-ε)	Surface average (Spalart-Allmaras)
Grid E	101336	314313	108731	5.63 MPa	6.17 MPa
Grid F	131425	382725	152792	5.76 MPa	6.33 MPa
Grid G	152942	422768	186765	5.62 MPa	6.21 MPa

C. Grid distribution

Grid distribution uses the Star-CCM+ program's built-in mesh generator, along with the trimmer, surface remesher, and prism layer meshing models. In addition, we have used a two-layer prism component and a block having a base size of only 0.00002 m. Refined meshing was applied to the region around the flapper's V-groove to improve accuracy. There are 131425 cells, 382725 faces, and 152792 vertices, which are shown in Fig. 3. Fig. 3(a) shows mesh model of the pilot stage and 3(b) represents the derived part of the pilot stage.

The precision of convergence is 1×10^{-5}. You may create orthogonal prismatic cells near the edges of walls by combining the prism layer's mesh. A mesh system's maximum skewness angle is one of the key metrics for gauging its quality. A skews angle of 90 degrees or greater is problematic in STAR-CCM+ and can occur in concave cells. According to Fig. 4, every single study ensures that the majority of the skewness angle remains below 45 degrees.

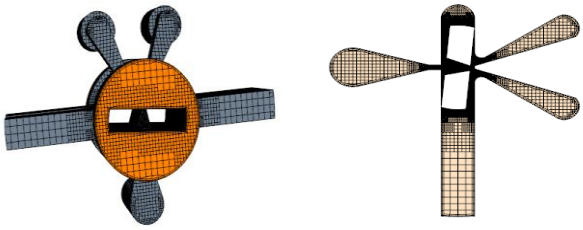

(a) Mesh model **(b) Derived part**

Fig. 3. Meshing model of the deflector jet pilot stage and its plane section.

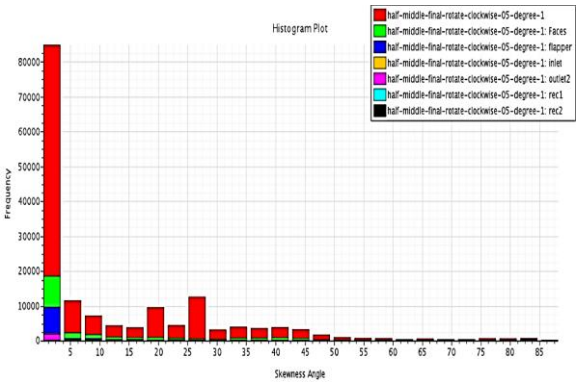

Fig. 4. Histogram of skewness angle.

D. Rationale for turbulence model selection

Two different turbulence models have been selected to account for the particularities of a malfunctioning DJSV. The Spalart-Allmaras model is a one-equation model that solves a transport equation for the modeled turbulent eddy viscosity. It was chosen because it has proven reliable in aerospace applications involving wall-bounded flow and adverse pressure gradient. At an inclined angle in the V-groove, this occurs when the jet strikes the groove at an oblique angle, leading to local flow separation. The Spalart-Allmaras model is computationally efficient and uniquely designed to account for layer offsets at the boundaries, where two-equation models overdo turbulence. Further, realizable $k-\varepsilon$ was selected because it introduces a dissipation rate term in the turbulent transport equation and a critical coefficient that varies with the mean flow and turbulence characteristics. Higher curvature and rotation can be found in the flow of a malfunctioning servo-valve with a 5-degree malfunction. Specifically, the realizable formulation addresses all these conditions better than the usual $k-\varepsilon$ model, thereby ensuring the mathematical consistency (realizability) of the normal stresses.

E. Boundary conditions

In Fig. 2, we can see the design that dictates the boundary conditions of the servo-valve construction. The input, wall, and output boundaries are the three types of boundaries that define the computational domains. All other surfaces have wall-type boundaries that demarcate the regions around the fluid or solid. The presence of viscous flow automatically enforces the no-slip wall criterion. Temperature changes are not considered. The inlet boundary condition of pressure is defined as the supply point. Pressure acts on the amplifier's upper and lower surfaces. There is a pressure differential of 20 MPa to 24 MPa at the input and 1 MPa at the output.

Result and Discussion

This section analyzes the pressure and velocity distribution of a servo-valve for a 5-degree rotational malfunction. This work compares the realizable k-ε model and Spalart-Allmaras turbulence models to better understand how they capture flow-induced changes. The effects of varying supply pressure on pressure distribution, velocity patterns, and system response are studied to highlight model-specific performance.

A. Pressure distribution

When the supply pressure rises from 20 MPa to 24 MPa, the pressure of receivers A and B increases. Because the greater supply pressure drives more fluid into the servo-valve, pressure throughout the system increases. Also, it is notable that the effective orifice size decreases when the flapper is at 5 degrees clockwise; pressure drops in receiver B and increases in receiver A. The Spalart-Allmaras model generates more pressure in receiver A than the realizable k-ε model. This demonstrates the Spalart-Allmaras model's capacity to capture turbulence and flow separation in high-pressure environments. Particularly in places where the flow has significant rotation and complicated behavior, the Spalart-Allmaras model offers a more comprehensive result of turbulent viscosity than the realizable k-ε model. The model correctly forecasts localized high-pressure zones as supply pressure rises, generating higher pressures in receiver A. This observation is shown in Fig. 5.

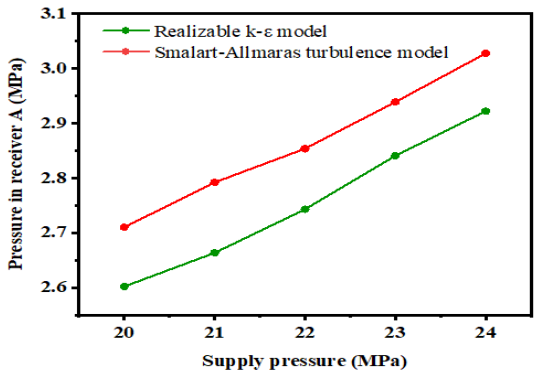

Fig. 5. Comparison of pressure distribution in receiver A for Spalart-Allmaras and realizable k-ε models.

The realizable k-ε model has a higher pressure than the Spalart-Allmaras model in receiver B. The realizable k-ε model is well-suited to handling complex flow dynamics and pressure losses because it imposes additional constraints that ensure the turbulence representation remains realistic. Its equation structure enables more accurate modeling of pressure decreases and flow stability, particularly in areas with complex interactions. As supply pressure increases, this model better captures the intricacies of fluid behavior, leading to higher pressure measurements in receiver B, as shown in Fig. 6.

For both the Spalart-Allmaras and realizable k-ε models, analyzing the scalar scene of pressure distribution is crucial. It physically shows how pressure varies across valve surfaces and helps identify localized high-pressure zones, flow separation, and turbulence.

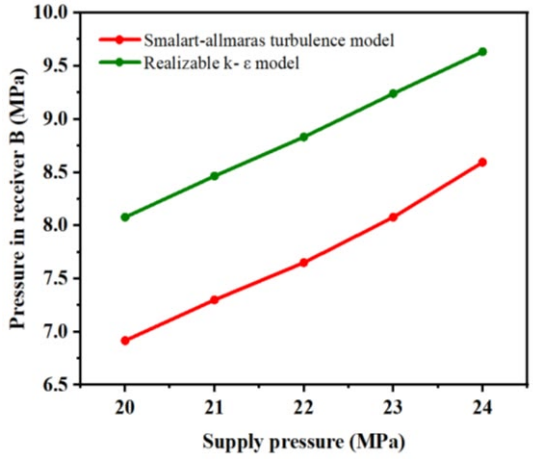

Fig. 6. Comparison of pressure distribution in receiver B for Spalart-Allmaras and realizable k-ε models.

At a traditional neutral position (without malfunction), the pilot stage of the DJSV is in a state of complete hydrodynamic symmetry. The jet of supply leaving the nozzle impacts directly on the shunt wedge, thus creating a stagnation point in the center of the fluid, which converts the kinetic energy of the fluid into a static pressure. Since the geometry is perfectly aligned, the pressure field is reflected with respect to the vertical axis of the valve. As a result, the pressure recovery in the two receivers is equivalent, resulting

in a zero differential pressure as shown in Fig. 7(c) (Saha et al., 2024). The pressure gradients in this regime are smooth and predictable, and there are no localized regions of low pressure commonly referred to as hot spots, indicative of flow separation or cavitation. Although the traditional setup maintains a balanced pressure field, the addition of a 5-degree malfunction introduces complex non-linear pressure remnant changes that require a dual-model verification. The Spalart-Allmaras model is used to trace the adverse pressure gradient and the likely separation at the receiver walls due to the steep angle of impingement, which direct effects the efficiency of pressure recovery. At the same time, the realizable k-ε model is also essential for addressing streamline curvature and rotational pressure variation in the V-groove, as mathematical restrictions limit the over-representation of turbulence kinetic energy in swirling flow.

Comparing the scalar landscapes of different models reveals how each forecast behaves and experiences turbulence under similar conditions, thereby informing model selection for maximum performance in hydraulic systems. The scalar scene of pressure distribution is shown in Figs. 7(a) and 7(b).

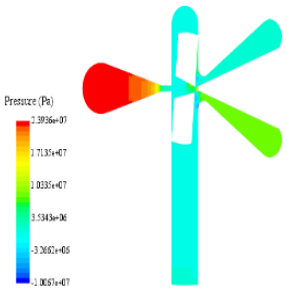

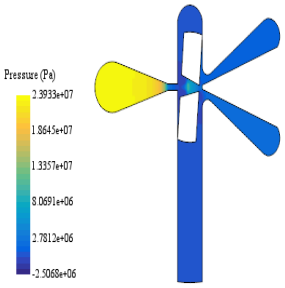

(a) Spalart-Allmaras **(b) Realizable k-ε**

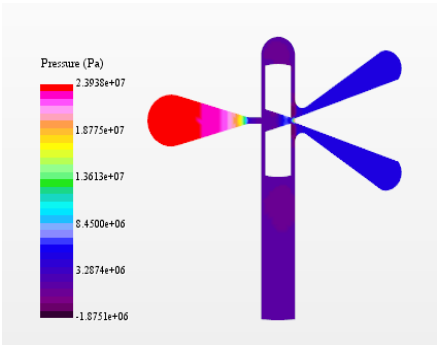

(c) Middle flapper position for the traditional model.

Fig. 7. Scaler scene of pressure distribution.

Also, pressure in the cross-sectional area for both models has been calculated and compared with the traditional model (Saha et al., 2024) to understand how fluid forces distribute within the valve, as illustrated in Fig. 8.

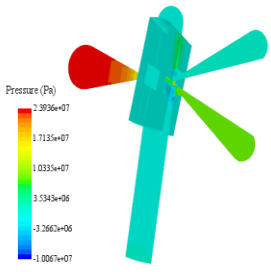

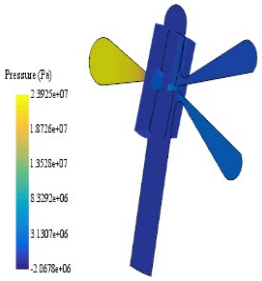

(a) Spalart-Allmaras **(b) Realizable k-ε**

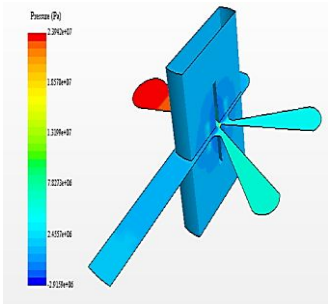

(c) Traditional model

Fig. 8. Pressure comparison in the cross-sectional area.

To sum up, the differences between the models are clearly important relative to the traditional neutral position, where the two models agree on the same outcomes because of a symmetrical, predictable flow-field and no separation. Nevertheless, when

the state becomes malfunctioning, the symmetry that is broken sparks two different phenomena requiring the application of different mathematical approaches. The models that forecast high pressure in Receiver A include the Spalart-Allmaras model, which is designed to solve only wall-bounded flow; thus, it successfully predicts the stagnation pressure at the rear part of the jet striking the inlet at an acute angle. On the other hand, the realizable k-ε model is more stable in the shadow areas of Receiver B due to the realizability constraint, which prevents excessive generation of turbulent kinetic energy in the rotating vortices developed within the V-groove. It shows that to measure the entire extent of performance deterioration in a malfunctioned valve, a dual-model method is necessary.

B. Surface average

Increasing supply pressure from 20 MPa to 24 MPa in a servo-valve system increases surface average pressure according to the Spalart-Allmaras and realizable k-ε turbulence models. This increase is caused by higher fluid energy in the system resulting from increased supply pressure. The motion of the fluid increases with increasing pressure, thereby generating greater force on the surfaces of the valve. As the fluid moves through the system, these dynamics raise average surface pressures. In high-pressure conditions, the Spalart-Allmaras model more precisely forecasts turbulent viscosity and flow dynamics than the realizable k-ε turbulence model. Therefore, it produces a surface average pressure higher than that of the realizable k-ε turbulence model. Particularly in regions with significant areas of high rotation and separation, the Spalart-Allmaras model effectively captures the complex interactions in turbulent flows, thereby producing significant surface pressure build-up, as shown in Fig. 9.

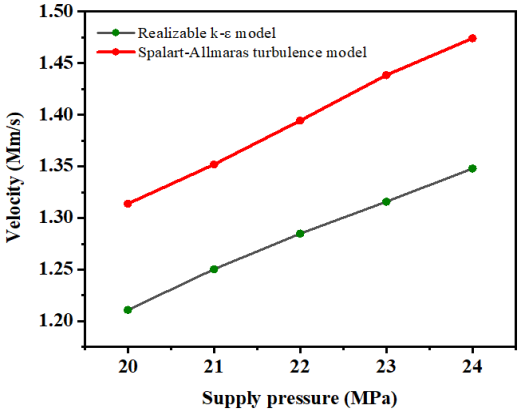

Fig. 9. Comparison of surface average for Spalart-Allmaras and realizable k-ε models.

C. Velocity distribution

Increasing supply pressure increases fluid velocity in both models, as flow rate and pressure are strongly related to velocity. Increased pressure from 20 to 24 MPa accelerates the fluid through the valve orifice. The Spalart-Allmaras turbulence model exhibits greater velocity while the supply pressure is increased, as illustrated in Figure 10. This is because this model better captures flow separation and rotational effects. The split-Allmaras turbulence model provides a finer resolution of turbulent viscosity near walls and therefore simulates fast, confined flow patterns more accurately than the realizable k-ε model, which averages turbulence effects over a larger region.

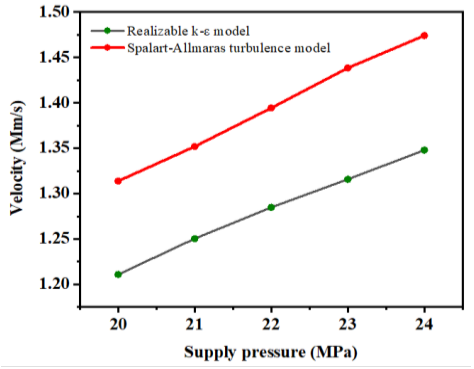

Fig. 10. Comparison of velocity distribution for Spalart-Allmaras and realizable k-ε models.

To visualize flow patterns and velocity variations across different models, scalar and vector scenes of the velocity distribution shown in Figs. 11 and 12,

respectively, compared with the traditional middle position of the flapper (Saha et al., 2024). During the neutral position of the flapper, the velocity field is observed to be entirely symmetrical, with the jet core cutting in half at the shunt wedge, thus yielding an equilibrium kinetic energy distribution. The emergence of the malfunction, however, involves the comparative implementation of two turbulence models, which are considered because they cause the otherwise stable jet to become a highly non-linear flow field with skewed momentum flux and centrifugal influence. Physically, the failure forces the jet to hit the receiver wall at an oblique angle, creating a high- velocity impingement zone unique to each model. The Spalart-Allmaras model is essential for solving steep velocity gradients and fully describing boundary-layer attachment at the receivers. On the other hand, the realizable k-ε model is to correctly capture rotational energy and streamline curvature, as the fluid is driven into the V-groove. With the assistance of both models, it is possible possible to verify the theoretical velocity losses in the receivers.

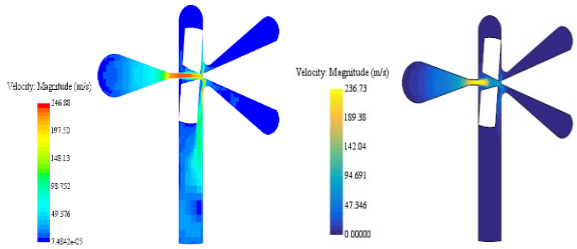

(a) Spalart-Allmaras **(b) Realizable k-ε**

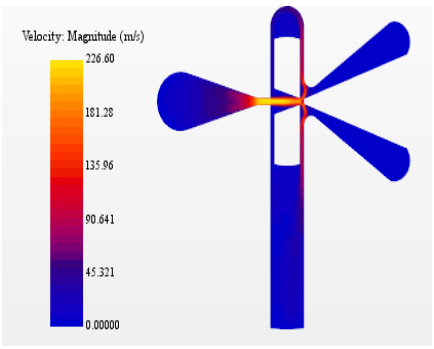

(c) Middle position without malfunction.

Fig. 11. Scalar scene of velocity distribution.

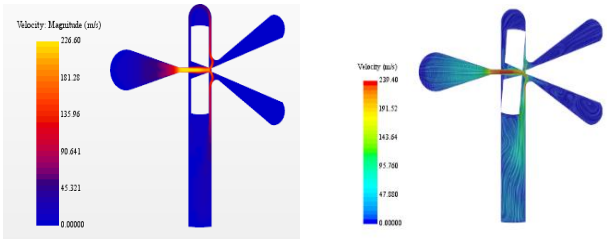

(a) Spalart-Allmaras **(b) Realizable k-ε**

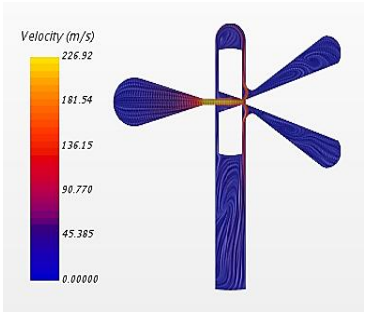

(c) Middle position without malfunction for the traditional model

Fig. 12. Vector scenes of velocity distribution.

Moreover, to visualize both the magnitude and direction of flow, vector contour for both models are shown in Fig.13.

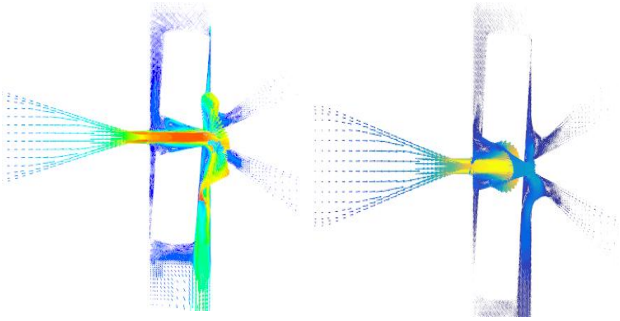

(a) Spalart-Allmaras **(b) Realizable k-ε**

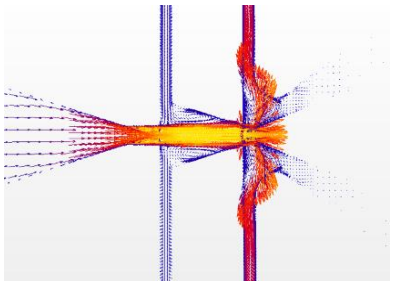

(c) Traditional models for neutral flapper positions.

Fig. 13. Vector contour of velocity distribution.

Also, velocity across the cross-sectional area is observed in both models, as illustrated in Fig. 14.

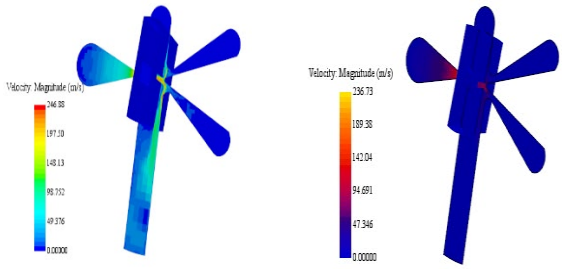

(a) Spalart-Allmaras **(b) Realizable k-ε**

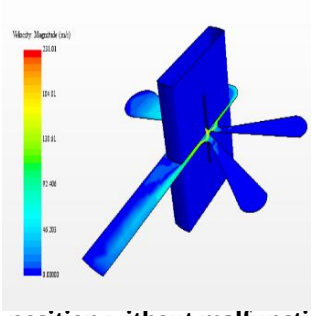

(c) Middle position without malfunction for the traditional model

Fig. 14. Velocity comparison of cross-sectional area.

Implementation of the study

This study provides a key finding: selection models of turbulence to analyze the operation of electro-hydraulic servo-valves (EHSV) under specified malfunctioning conditions. This result emphasizes the relationships among several significant physical parameters in deflector-jet servo-valves (DJSVs) during malfunction, and these results are beneficial for computational fluid dynamics (CFD) methods. Specifically, the supply pressure is directly related to the jet velocity, which, in turn, amplifies the pressure distributions and creates an asymmetry between receivers A and B with increasing deflector angle. Boundary-layer effects do control the shape of the velocity profiles, amplifying kinetic energy and decreasing it in V-grooves than in nozzles, and hence correlate with differences in pressure, which lead to spool movement and systems reliability. The intensity of turbulence varies the effective viscosity; high supply pressure increases the effect of jet forces and oscillations, a point that shows some correlatability with erosion alleviation in the air aircraft scenario. The implications of this study state the relationship of supply pressure, jet velocity, and pressure asymmetry in the DJSVs, where the model-specific abilities are reflected: the Spalart-Allmaras model is well equipped to deal with wall-bounded velocity fields, whereas the realizable k-ε model is more competent in shear-driven losses and can help in the model selection of accurate malfunctioning prediction. The application of such results to broader processes involves optimizing resistance to contamination and the dynamical response, as the revealed parameter relationships can be used to improve the design of the model, such as altered nozzle shapes, to achieve flow equilibrium. In the field of mechanical engineering, the results are valuable for predictive maintenance strategies, as they establish a correlation between supply pressure and vibrations caused by uneven pressure distribution.

Despite the detailed comparison of the two analyses, the current study has several limitations. First, the research is only focused on a specific malfunction condition; as such phenomena are caused by flow, they are not studied at other angles. Secondly, whereas the pressure and velocity differences are described, the effects of cavitation, which is often involved in erosion and noise disturbances in DJSVs, are not measured. In addition, the thermal effects and the full interaction between the pilot and main stages have not been considered in the simulation due to a simplified geometry model, prioritizing pilot-stage fidelity over increased computational efficiency. In future studies, multiphase cavitation modeling and thermal analysis will be needed to provide a more comprehensive representation of servo-valve failure modes.

Conclusion

We analyzed pressure distribution, surface-average, and velocity distributions using the Spalart-Allmaras and realizable k-ε turbulence models for a 5-degree clockwise servo-valve malfunction. The goal was to investigate how each model captured flow behavior and turbulence under varying supply pressures and rotational movements. For the increase of supply pressure, pressure in receivers A and B increases for

both the Spalart-Allmaras and the realizable k-ε turbulence model. Moreover, for a 5-degree malfunction, the Spalart-Allmaras model shows higher pressure in receiver A when the supply pressure increases due to better handling of flow separation. However, the realizable k-ε model captures pressure more effectively in receiver B, likely due to differences in turbulence averaging. Both models show an increase in surface average as supply pressure increases. The Spalart-Allmaras model produces higher surface averages, reflecting its better ability to anticipate localized flow changes.

Increased supply pressure increases fluid velocity in both models. The Spalart-Allmaras model exhibits higher velocities when the supply pressure is increased due to improved resolution of rotational effects and wall-bound flows.

Acknowledgment

The following support is gratefully acknowledged: Professor Songjing Li, Head of the Department of Fluid Control and Automation, Harbin Institute of Technology (HIT), Harbin, China, and the National Natural Science Foundation of China (No. 51675119).

Authors contribution

Md Shah Najmus Shakib: Conceptualization; methodology; software; validation; visualization; investigation; drafting the original manuscript; revision; formal analysis. Bijan Krishna Saha: Supervision; critical review and editing; original manuscript; formal analysis; validation; software; visualization.

Conflict of interest

The authors have no financial or personal relationships that could have influenced the study.

References

Saha BK, Peng J and Li S. Numerical and experimental investigations of cavitation phenomena inside the pilot stage of the deflector Jet Servo-Valve, *IEEE Access*, 2020; 8: 64238-64249.

Gao D. Finite element numerical simulation and PIV measurement of the flow field inside metering-in spool valve. *Chin. J. Mech. Eng.* 2009; 22(1): 102-108.

Abdallah HK, Peng J and Li S. Analysis of pressure oscillation and structural parameters on the performance of deflector jet Servo-valve. *Alex. Eng. J.* 2023a; 63: 675-692.

Abdallah HK, Ben-Mansour R and Li S. Numerical study of erosion phenomena with the presence of cavitation at deflector jet servo-valve. *Arab. J. Sci. Eng.* 2023b; 49(2): 15.

Yan H, Li J, Cai C and Ren Y. Numerical investigation of erosion wear in the hydraulic amplifier of the deflector jet Servo-valve. *Appl. Sci. (Switzerland)*, 2020; 10(4): 1299.

Yan H, Ren Y, Yao L and Dong L. Analysis of the internal characteristics of a deflector jet servo-valve. *Chin. J. Mech. Eng.* 2019; 32: 31.

Yang H, Wang W and Lu K. Cavitation and flow forces in the flapper-nozzle stage of a hydraulic servo-valve manipulated by continuous minijets. *Adv. Mech. Eng.* 2019a; 11(5): 168781401985143.

Yang H, Wang W and Lu K. Numerical simulations on flow characteristics of a nozzle-flapper Servo-valve with diamond nozzles. *IEEE Access*, 2019b; 7: 28001-28010.

Yang H, Wang W, Lu K and Chen Z. Cavitation reduction of a flapper nozzle pilot valve using continuous microjets. *Int. J. Heat Mass Transf.* 2019c; 133:1099-1109.

Sandor IB and Suan-Resiga R. Numerical model for cavitational flow in Hydraulic poppet valve. *model. Simul. Eng.* 2012; 2012: 742162.

Chen J, Li F, Yang Y and Gao Y. Mathematical modelling and hierarchical encourage particle swarm optimization genetic algorithm for jet pipe servo-valve. *Comput. Intell. Neurosci*. 2022; 2022(7): 9155248.

Liang J, Luo X, Liu Y, Li X and Shi T. A numerical investigation in effects of inlet pressure

fluctuations on the flow and cavitation characteristics inside water hydraulic poppet valves.*Int. J. Heat Mass Transf.* 2016; 103: 684-700.

Saha BK, Peng J, Shakib MSN, Li S and Jihan JI. A numerical analysis of pressure characteristics in the deflector jet pilot stage valve with an innovative deflector deflection. *Flow Meas. Instrum.* 2024; 99: 102674.

Zou J, Fu X, Du XW, Ruan XD, Ji H, Ryu S and Ochiai M. Cavitation in a non-circular opening spool valve with U-grooves. *Proc. Inst. Mech. Eng. A, J. Power Energy*, 2008; 222(4): 413-420.

Jacob M, Mchenya S, Zhang and Li S. A study of flow-field distribution between the flapper and nozzle in a hydraulic servo- valve.In:*Proc. Int. Conf. Fluid Power Mechatronics, Beijing, China*, 2011; pp. 658-662.

Wu L, Chen K and Zhan C. Snapshot POD analysis of transient flow in the pilot stage of a jet pipe Servo-valve. *J. Turbulence*, 2018; 19(10); 889-909.

Zhang L, Luo J, Yuan R and He M. The CFD analysis of twin flapper nozzle valve in pure water hydraulic. *Int. Conf. Adv. Comput. Model. Simul., Proc. Eng.* 2012; 31: 220-227.

Chen M, Aung NZ, Li S and Zou C. Effect of oil viscosity on self-excited noise production inside the pilot stage of a two-stage electrohydraulic servo-valve. *J. Fluids Eng.* 2019; 141(1): 011106.

Han M, Liu Y, Wu D, Zhao X and Tan H. A numerical investigation in characteristics of flow force under cavitation state inside the water hydraulic poppet valves. *Int. J. Heat Mass Transf.* 2017; 111: 1-16.

Aung NZ and Li S. A numerical study of cavitation phenomenon in a flapper- nozzle pilot stage of an electrohydraulic servo-valve with an innovative flapper shape. *Energy Convers. Manage.* 2014; 77:31-39.

Tamburrano P, Plummer AR, Distaso E and Amirante R. A review of electrohydraulic servo-valve research and development. *Int. J. Fluid Power*, 2018; 201: 53-98.

Tamburrano P, Plummer AR, Palma PD, Distaso E and Amirante R. A novel servo-valve pilot stage actuated by a piezo-electric ring bender: A numerical and experimental analysis. *Energies*, 2020; 13(3): 671.

Yang Q, Aung NZ and Li S. Confirmation on the effectiveness of rectangle-shaped flapper in reducing cavitation in flapper–nozzle pilot valve. *Energy Convers. Manage.*, 2015; 98: 184-198.

Li S, Aung NZ, Zhang S, Cao J and Xue X. Experimental and numerical investigation of cavitation phenomenon in flapper–nozzle pilot stage of an electrohydraulic servo-valve. *Comput. Fluids*, 2013; 88: 590-598.

Chu Y, Yuan Z and Chang W. Research on the dynamic erosion wear characteristics of a nozzle flapper pressure servo-valve used in aircraft brake system. *Math. Probl. Eng.* 2020; 2020: 136412.

Chu Y, Yuan Z, He X. and Dong Z. Model construction and performance degradation characteristics of a deflector jet pressure servo-valve under the condition of oil contamination. *Int. J. Aerosp. Eng.* 2021; 2021(5): 8840084.

Ren Y, Yan H, Mao Q, Zuo Z and Hao H. A model-based investigation of the performance robustness of the deflector jet servo-valve. *Appl. Sci.* 2022; 12(20): 10428.